Microporous and Mesoporous Materials 190 (2014) 152–155

Contents lists available at ScienceDirect

Microporous and Mesoporous Materials

journal homepage: www.elsevier.com/locate/micromeso

A high-performance adsorbent for hydrogen sulfide removal

Bahman Elyassi [a], Yasser Al Wahedi [a,b], Nafiseh Rajabbeigi [a], Prashant Kumar [a], Jong Seok Jeong [a], Xueyi Zhang [a], Parveen Kumar [a], Veerappan V. Balasubramanian [a], Marios S. Katsiotis [b], K. Andre Mkhoyan [a], Nikos Boukos [c], Saleh Al Hashimi [b], Michael Tsapatsis [a,*]

[a] Department of Chemical Engineering & Materials Science, University of Minnesota, Minneapolis, MN 55455, USA
[b] Department of Chemical Engineering, Petroleum Institute, P.O. Box 2533, Abu Dhabi, United Arab Emirates
[c] Institute of Advanced Materials, Physicochemical Processes, Nanotechnology and Microsystems (IAMPPNM), Division of Physical Chemistry, National Center for Scientific Research "Demokritos", Athens, Greece

ARTICLE INFO

Article history:
Received 9 September 2013
Received in revised form 23 January 2014
Accepted 4 February 2014
Available online 12 February 2014

Keywords:
Hydrogen sulfide adsorbent
Regeneration
SBA-15
Copper-zinc oxides
Claus process

ABSTRACT

Spatially well-distributed copper-zinc oxides supported on mesoporous silica (SBA-15 and commercial silica gel) showed high adsorption capacity for hydrogen sulfide (as high as 80 mgS/$g_{sorbent}$) and stability during cyclic adsorption-regeneration process.

1. Introduction

Developing more efficient technologies to capture hydrogen sulfide (H_2S) has been under intense investigation to alleviate the negative environmental impact of processing and utilization of fossil-based resources. Currently, once-through adsorbents (mostly zinc-based) are widely used in ammonia, methanol, and hydrogen plants to protect catalysts. H_2S removal in several processes (e.g., to avoid the poisoning effect of sulfur on catalysts and fuel cell electrodes, and for use in small foot-print capture technologies for oil and natural gas processing units) favors developing regenerable solid sorbents. However, low adsorption capacity of commercial solid adsorbents requires large bed volume while frequent landfilling of spent adsorbents is of major environmental concern [1]. Factors such as grain growth, sorbent underutilization due to diffusion-limited gas–solid reaction, mechanical attrition, and formation of thermodynamically stable and non-regenerable side products have been suggested as the leading causes for loss of performance in metal oxide-based adsorbents [2]. Zinc and copper oxides supported on mesoporous silica have attracted recent attention for H_2S capture due to potential for combination of favorable sulfidation thermodynamics with highly dispersed active metal oxides [1,3–6]. Recently, de Jongh and co-workers showed that Cu-ZnO nanoparticles, with near-maximum inter-particle distance supported on porous silica, exhibit significantly enhanced stability as a catalyst for methanol synthesis [7]. Based on this development, we hypothesized that spatially well-distributed active metal oxides or mixed metal oxides on mesoporous hosts can also be highly stable during H_2S adsorption-regeneration cycles. Here, we demonstrated such stability coupled with high H_2S adsorption capacity of silica-supported copper-zinc oxides.

2. Experimental

Mesoporous silica SBA-15 [8] was synthesized according to the procedure developed by Sayari et al. [9]. Porous silica gel was acquired from Sigma–Aldrich (high-purity grade, Davisil Grade 635, pore size 60 Å, 60–100 mesh, pore volume = 0.75 ml/g). Cu-ZnO-SBA-15 and Cu-ZnO-Silica gel (SG) were synthesized by incipient wetness impregnation of 4 M aqueous solution of $Cu(NO_3)_2{\cdot}3H_2O$ and $Zn(NO_3)_2{\cdot}6H_2O$ (molar ratio Cu:Zn = 2:1). 1.0 ml and 0.75 ml of the above solution were added to 1 g SBA-15 and 1 g silica gel in 0.2 ml batches, respectively. For comparison purposes, CuO-SBA-15 and ZnO-SBA-15 were prepared using the above procedure by impregnating 1 g SBA-15 with 1.0 ml of the corresponding solution. Drying and calcination were performed according to Prieto et al. [7] with some minor modifications: after impregnation, powders were vacuum dried at room temperature for 1 day and then were calcined at 500 °C

* Corresponding author. Tel.: +1 (612) 626 0920.
E-mail address: tsapatsis@umn.edu (M. Tsapatsis).

http://dx.doi.org/10.1016/j.micromeso.2014.02.007
1387-1811/

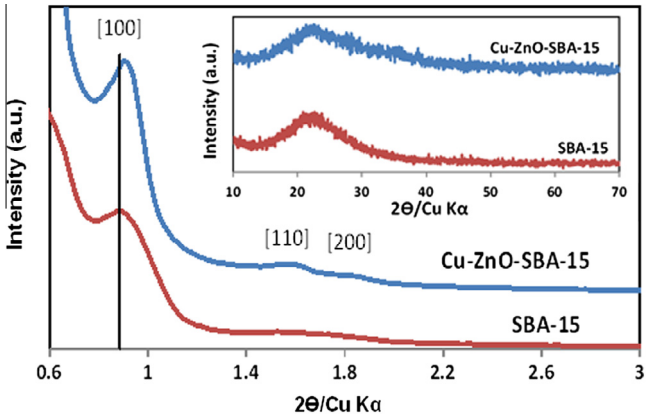

Fig. 1. Low angle XRD patterns of SBA-15 and Cu-ZnO-SBA-15. Inset shows wide angle patterns.

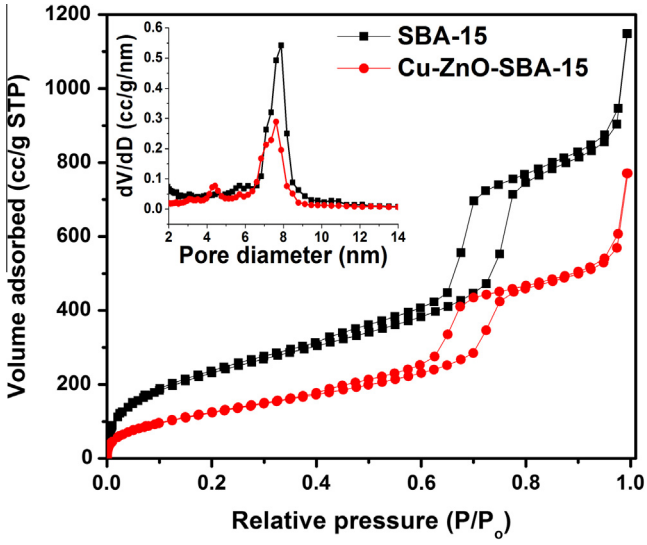

Fig. 2. Argon adsorption–desorption isotherms: SBA-15(■) and Cu-ZnO-SBA-15(●); measured at 87 K. Pore size distribution (inset) was obtained using NLDFT [14] (silica, cylindrical pores).

for 4 h under a nitrogen flow of 50 ml/min in an alumina boat placed in a tubular furnace.

The experimental set-up for sulfidation-regeneration studies was constructed from stainless steel 316 tubing and connections. 15 mg of adsorbent was diluted with 0.3 g of quartz powder (mesh 40–80) and sandwiched between quartz wool plugs in a U-shaped quartz tube of 4 mm inside diameter. Adsorbents were dried under helium flow at 300 °C for 3 h and then were exposed to an H_2S containing stream of 42 ml/min (102 ppmv in He, Praxair) at 150 °C and 1 atm. The H_2S concentration at the reactor exit was monitored on-line using a gas chromatograph (Agilent 7890A) equipped with a sulfur chemiluminescence detector (SCD). Breakthrough capacity was determined at an exit H_2S concentration equal to 5% of the inlet. Regeneration was conducted by sequential oxidation–reduction of the sulfidated adsorbent in the same reactor for five times. Oxidation was performed at 400 °C for 0.5 h with a 50 ml/min flow of 5% O_2 (in balance N_2), and reduction at 400 °C for 1 h with a 50 ml/min flow of 10% H_2 (in balance He). After the fifth reduction, the adsorbent was activated with another oxidation step. The reactor was flushed with helium in between for safety reasons.

The powder XRD measurements were carried out using a Bruker-AXS (Siemens) D5005 diffractometer with a CuKα ($\lambda = 0.15406$ nm) radiation source. Argon adsorption–desorption isotherms were obtained using a Quantachrome Autosorb-1 instrument at 87 K. Samples were degassed at 300 °C for 5 h under vacuum prior to the analysis. The pore size distributions were obtained from the adsorption branch of the isotherms using the nonlocal density functional theory (NLDFT) method (Quantachrome software, version 1.11) [14]. HAADF-STEM imaging was performed at 300 kV with an incident semi-convergent angle of 21.4 mrad and detector collection angles of 58.5–200 mrad on an FEI Titan™ G2 60–300 scanning transmission electron microscope (STEM). SBA-15 powder was sprinkled directly on carbon supported molybdenum grid for imaging. Cu-ZnO-SBA-15 and its sulfidated form was embedded in resin, microtomed into 60–100 nm thin electron transparent sections and placed on the grid.

3. Results and discussion

XRD patterns of SBA-15 and Cu-ZnO-SBA-15 (Cu:Zn:Si with a nominal molar ratio of 2:1:12.5) confirm formation of mesoporous

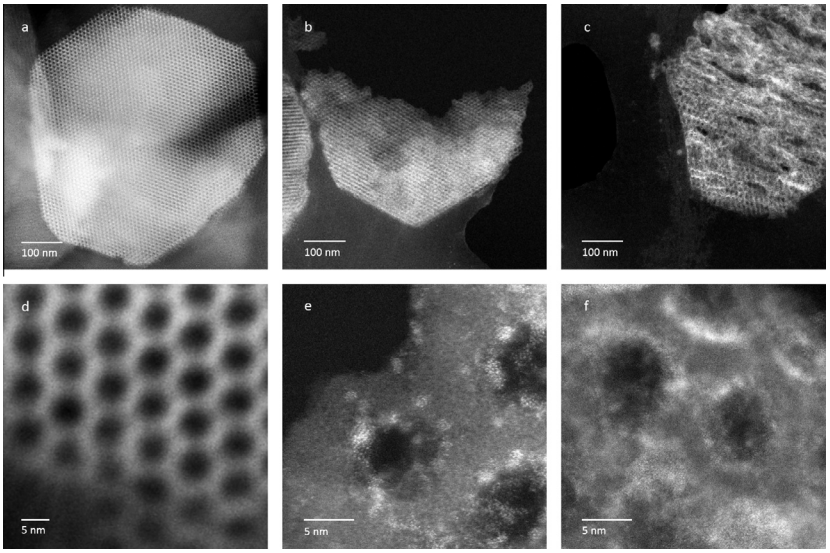

Fig. 3. Low- and high-magnification HAADF-STEM images of SBA-15 (a, d), Cu-ZnO-SBA-15 (b, e), and sulfidated Cu-ZnO-SBA-15 (c, f). Highly dispersed nanoparticles can be seen in Cu-ZnO-SBA-15 before and after sulfidation.

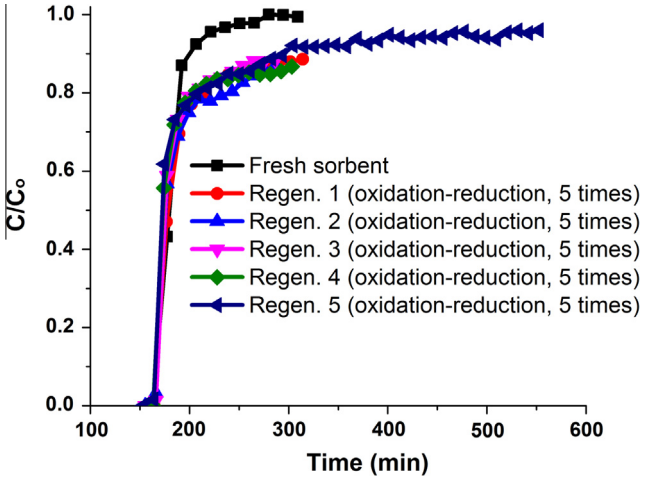

Fig. 4. H_2S breakthrough curves from cyclic adsorption-regeneration tests of Cu-ZnO-SBA-15 at 150 °C with H_2S (102 ppmv in He) followed by sequential oxidation (400 °C, 0.5 h (5% O_2 in N_2)) – reduction (400 °C, 1 h (10% H_2 in He)) for five times. After the fifth reduction, the adsorbent was activated by oxidation at 400 °C, 0.5 h (5% O_2 in N_2).

silica and its structural stability after incorporation of copper and zinc oxides (see Fig. 1). After incorporation of oxides, the characteristic reflections shifted slightly (0.2 nm) to higher angles, indicating framework contraction. No peak associated with copper or zinc oxides can be detected in the diffraction patterns of Cu-ZnO-SBA-15 nor in Cu-ZnO-SG; suggesting high dispersion of incorporated nanoparticles [4,10–12]. Ar adsorption isotherms (Fig. 2) are type IV with H1 hysteresis; consistent with SBA-15 [13]. The cumulative pore volume obtained using NLDFT method [14] decreased from 1.34 ml/g to 0.77 ml/g which can be attributed to the presence of nanoparticles in the pores. Also, embedding nanoparticles in SBA-15 resulted in a reduction in the median pore size from 7.9 nm to 7.6 nm.

The HAADF-STEM images of SBA-15, Cu-ZnO-SBA-15, and sulfidated Cu-ZnO-SBA-15 are shown in Fig. 3. SBA-15 shows hexagonal particle morphology with the pore diameter of about 8 nm. HAADF-STEM images have characteristic Z-contrast [15] with heavier atomic columns appearing bright in the image. Bright clusters <3 nm diameter are uniformly distributed throughout the particles of the adsorbent before (Cu-Zn-O) and after sulfidation (Cu-Zn-S). Through focal series across the pore depth inclined at an angle to the electron beam revealed that the clusters are supported on the pore walls (not shown here).

Cu-ZnO-SBA-15 when exposed to H_2S (102 ppmv in He) at 150 °C showed breakthrough capacities as high as of 75 mgS/$g_{sorbent}$. Elemental analysis using Inductively Coupled Plasma-Atomic Emission Spectrometry (ICP-AES, by Galbraith Laboratories, Inc.) showed loadings of 11.2 and 6 wt% for Cu and Zn, respectively. The theoretical saturation capacity, therefore, was calculated to be 86 and 58 mgS/$g_{sorbent}$ (assuming sulfidation to CuS–ZnS or Cu_2S–ZnS, respectively). Assuming copper oxide and zinc oxide were fully converted to CuS and ZnS, sorbent utilization capacities as high as 87% was obtained.

A typical behavior of the adsorbent to cyclic adsorption-regeneration is presented in Fig. 4. The adsorbent was regenerated using a sequence of oxidation (400 °C, 0.5 h (5% O_2 in N_2)) – reduction (400 °C, 1 h (10% H_2 in He)) for five times and as shown in Fig. 4 the adsorbent was fully regenerable. It should be noted that the reduction step was used to reduce the copper sulfate that was formed during the oxidation step [16]. A final oxidation step in the sequence was applied to activate the adsorbent by converting copper to copper oxide. After the first regeneration, the breakthrough curves leveled off at $C/C_0 = 1$ but at a slower pace, suggesting a change in the kinetics of adsorption process. Elemental analysis of the sulfidated Cu-ZnO-SBA-15, after one time oxidation, and after five times of oxidation–reduction showed sulfur contents of 17.2 mgS/$g_{sorbent}$, and 7.6 mgS/$g_{sorbent}$, respectively. This indicates that the combination of oxidation and reduction for regeneration can be effective in reducing the retention of sulfur species on the adsorbent. After one oxidation 25% of sulfur remains, while

Table 1
A performance summary for the state-of-the-art silica-supported copper and zinc oxides in the literature.

Adsorbent	Breakthrough capacity (mgS/$g_{sorbent}$)	Utilization%	T (°C)	Refs.
11.2%Cu-6%Zn-SBA-15	75	87	150	This work
10.6%Cu-5%Zn-SG	34	44		
ZnO-15%-MCM-41	9.6	16	25	[1]
ZnO-15%-KIT-6	9.1	12		
ZnO-15%-SBA-15-Sphere	21.1	36		
ZnO-15%-SBA-15-Fiber	21.8	37		
ZnO-3%-TNP (TiO_2 NP)	5.0	42		
ZnO-10%-ROZ3 (AC Norit)	8.0	20		
10%Cu-MSU-1	10.9	22	25	[3]
20%Cu-MSU-1	19.2	19		
30%Cu-MSU-1	19.4	13		
10%Zn-MSU-1	42.3	86		
20%Zn-MSU-1	14.8	15		
30%Zn-MSU-1	11.5	8		
Katalco (commercial)	Fresh 13–3[a]-3[b]	–	300	[4]
IWI-30%-500(ZnO-SBA-15)	Fresh 9–15[a]-18[b]	8		
TS-30%-500(ZnO-SBA-15)	Fresh 9–12[a]-12[b]	8		
ZnO (commercial)	Fresh 34.1–4.26[a]	–	20	[5]
ZnO-17%-SiO_2	Fresh 19.2–14.9[a]	21		
$Cu_{0.05}$-$ZnO_{0.95}$-SiO_2	Fresh 36.2–23.4[a] (saturation capacities)	41		
Cu38.5%-MCM-41	Fresh 30.9–25.8[a]-22.4[b]	32	515	[6]
Cu41.5%-MCM-41	Fresh 32.7–28[a]-26.5[b]	31		
Cu49.6%-MCM-41	Fresh 27.6–23.2[a]- 20.7[b]	22		

[a] After first regeneration.
[b] After second regeneration.

after the 5 oxidation–reduction cycles the remaining sulfur is reduced to about 10% of the adsorbed amount. This is important in suppressing sulfur dioxide emissions during the following adsorption cycle. These sulfur dioxide emissions are caused by the reduction of the remaining sulfate to sulfur dioxide by H_2S.

CuO-SBA-15 and ZnO-SBA-15 with the same loadings showed adsorption capacities of 80 $mgS/g_{sorbent}$ and 15 $mgS/g_{sorbent}$, respectively. Reactivity between zinc and silica and formation of zinc silicate [17] might explain the lower adsorption capacity of ZnO-SBA-15 than that of CuO-SBA-15. Further investigation is required to better understand what role each component plays.

Cu-ZnO supported on silica gel (a relatively inexpensive support material) was also examined. It exhibited a breakthrough capacity of 34 $mgS/g_{sorbent}$ for H_2S (102 ppmv in balance He). Note that the saturation capacities are 77 and 52 $mgS/g_{sorbent}$; depending on the assumed copper state of CuO or Cu_2O, respectively.

In comparison to other silica-supported copper and zinc adsorbents (Table 1), the adsorbents prepared according to the approach introduced by de Jong and co-workers [7] demonstrated enhancements in adsorption capacity and stability. Moreover, their performance in a simulated gas (H_2S 200 ppmv, CO 300 ppmv, C_2H_6 300 ppmv, CH_4 0.25%, Ar 0.59%, CO_2 19.88, N_2 79.2) remained unaffected (80 $mgS/g_{sorbent}$), indicating promise for industrial use in the tail gas treatment of the Claus process [18]. We envision that in this possible use the sulfur species generated during regeneration will be recycled to the feed of the Claus reactor. However, further tests of adsorption capacity under realistic feeds, optimization of the regeneration procedure, and process design studies are required to assess commercial feasibility.

4. Conclusions

Spatially highly-distributed mixed copper and zinc oxides on mesoporous silica hosts exhibit high sulfur capacity and are stable during H_2S adsorption-regeneration cycles.

Acknowledgements

This work was supported by ADGAS and GASCO, UAE. Parts of this work were carried out in the Characterization Facility, University of Minnesota, a member of the NSF-funded Materials Research Facilities Network (http://www.mrfn.org) via the MRSEC program. Electron microscopy characterization was supported by the MRSEC Program of the National Science Foundation under Award Number DMR-0819885.

References

[1] M. Hussain, N. Abbas, D. Fino, N. Russo, Chem. Eng. J. 188 (2012) 222–232.
[2] M. Behl, J. Yeom, Q. Lineberry, P. Jain, M. Shannon, Nat. Nanotechnol. 7 (2012) 810–815.
[3] D. Montes, E. Tocuyo, E. Gonzalez, D. Rodriguez, R. Solano, R. Atencio, M. Ramos, A. Moronta, Microporous Mesoporous Mater. 168 (2013) 111–120.
[4] M. Mureddu, I. Ferino, E. Rombi, M. Cutrufello, P. Deiana, A. Ardu, A. Musinu, G. Piccaluga, C. Cannas, Fuel 102 (2012) 691–700.
[5] H. Yang, B. Tatarchuk, AIChE J. 56 (2010) 2898–2904.
[6] O. Karvan, A. Sirkecioglu, H. Atakul, Fuel Process. Technol. 90 (2009) 1452–1458.
[7] G. Prieto, J. Zecevic, H. Friedrich, K. de Jong, P. de Jongh, Nat. Mater. 12 (2013) 34–39.
[8] D. Zhao, J. Feng, Q. Huo, N. Melosh, G. Fredrickson, B. Chmelka, G. Stucky, Science 279 (1998) 548–552.
[9] A. Sayari, B. Han, Y. Yang, J. Am. Chem. Soc. 126 (2004) 14348–14349.
[10] Q. Jiang, Z. Wu, Y. Wang, Y. Cao, C. Zhou, J. Zhu, J. Mater. Chem. 16 (2006) 1536–1542.
[11] Q. Lu, Z. Wang, J. Li, P. Wang, X. Ye, Nanoscale Res. Lett. 4 (2009) 646–654.
[12] Y. Wang, Z. Wu, L. Shi, J. Zhu, J. Adv. Mater. 17 (2005) 323–327.
[13] G. Laugel, J. Arichi, M. Moliere, A. Kiennemann, F. Garin, B. Louis, Catal. Today 138 (2008) 38–42.
[14] P. Ravikovitch, A. Neimark, Colloids Surf. A 187 (2001) 11–21.
[15] S.J. Pennycook, Ultramicroscopy 30 (1989) 58–69.
[16] K. Vo Van, F. Habashi, Can. J. Chem. Eng. 52 (1974) 369–373.
[17] O.P. Tkachenko, K.V. Klementiev, E. Löffler, I. Ritzkopf, F. Schüth, M. Bandyopadhyay, S. Grabowski, H. Gies, V. Hagen, M. Muhler, Lianhai Lu, R.A. Fischer, W. Grünert, Phys. Chem. Chem. Phys. 5 (2003) 4325–4334.
[18] P. Kumar, C. Sung, O. Muraza, M. Cococcioni, S. Al Hashimi, A. McCormick, M. Tsapatsis, Microporous Mesoporous Mater. 146 (2011) 127–133.